GRAIN DEFECT FORMATION DURING DIRECTIONAL

SOLIDIFICATION OF NICKEL BASE SINGLE CRYSTALS

T.M. Pollock*†, W.H. Murphy*, E.H. Goldman*, D.L. Uram** and J.S. Tu**

*Engineering Materials Technology Laboratories,
General Electric Aircraft Engines, Cincinnati, OH 45215
**Howmet Corporation, Whitehall, MI

†Present Address: Dept. of Materials Science & Engineering
Carnegie Mellon University, Pittsburgh, PA 15213

ABSTRACT

Grain defect formation during solidification of <001> nickel base single crystals has been studied in a series of alloys over a wide range of imposed thermal gradients and growth rates. Solute-driven convective instabilities, associated with high levels of Re and W and/or low levels of Ta, promote the formation of "freckle" defects as well as dendrite fragmentation and nucleation of misoriented grains. As the imposed positive thermal gradients at the solid-liquid interface decrease, grain nucleation events become more frequent until a general columnar to equiaxed transition is encountered. Transitions in solidification behavior and are shown to be consistent with changes in dendrite morphology and operative regimes of grain defect formation are characterized in terms of primary dendrite arm spacings.

INTRODUCTION

Single crystal turbine blades produced by directional solidification have led to dramatic improvements in engine performance. The complementary development of investment casting techniques for complex single crystal components and new alloys with higher melting points and uniform, creep resistant microstructures has led to large increases in the maximum temperature capabilities of turbine blades. However, as blade designs become more complex and refractory alloy content is increased for further improvement in creep properties, it is increasingly important to understand the influence of alloying additions on single crystal growth and the tendency for formation of grain defects during processing.

Several types of grain defects may develop during directional solidification [1]. Low angle boundaries and subgrains are common due to the dendritic character of the solidification process, but have no adverse effects on properties. High angle boundaries or equiaxed grains are however detrimental to mechanical properties and must be avoided, ideally through a combination of alloy design and careful control of the casting process. Highly misoriented grains may nucleate during directional solidification for any number of reasons, but it is not possible to predict how minor or even major changes in alloy composition influence grain nucleation. For a fixed alloy composition, it is also difficult to define processing parameters that prevent grain defect formation. In this research, the breakdown of single crystal solidification was studied in detail over a wide range of processing conditions in a series of high refractory content superalloys in order to gain a better understanding of the mechanisms of grain defect formation and the alloy/process conditions associated with their development.

EXPERIMENTAL ALLOYS AND PROCEDURES

Alloy compositions, listed in Table I, were selected to investigate a wide range of refractory alloying additions and to permit statistical analysis of results. Under fixed processing conditions <001> single crystals of each of these alloys were cast and defects in the directional dendritic structure due to the changing alloy content were studied in detail. Additionally, mechanisms of grain defect formation were investigated in Alloy SX-1 with experiments over a wide range of imposed thermal gradients (G) and solidification rates (R).

Table I - Nominal Composition of Experimental Single Crystal Alloys (Wt.%)

Alloy	Al	Cr	Co	Hf	Re	Ta	W	Ni
SX-1	6.0	4.5	12.5	0.16	6.3	7.0	5.8	Bal
SX-2	6.1	4.5	12.5	0.15	6.5	9.0	5.8	Bal
SX-3	5.7	4.0	11.5	0.12	5.0	6.0	5.0	Bal
SX-4	5.7	5.0	13.5	0.12	5.0	6.0	6.5	Bal
SX-5	6.3	4.0	13.5	0.18	6.5	6.0	5.0	Bal
SX-6	6.3	5.0	11.5	0.18	6.5	6.0	6.5	Bal
SX-7	6.3	5.0	11.5	0.12	5.0	9.0	5.0	Bal
SX-8	6.3	4.0	13.5	0.12	5.0	9.0	6.5	Bal
SX-9	5.7	5.0	13.5	0.18	6.5	9.0	5.0	Bal
SX-10	5.7	4.0	11.5	0.18	6.5	9.0	6.5	Bal

To achieve a wide range of processing conditions, crystals were investment cast in two different sample configurations in two different types of furnaces. First, individual cylindrical bars were directionally solidified in a modified Bridgman-type laboratory furnace capable of thermal gradients of 150°C/cm at the solidification front. To simulate conditions encountered in

single crystal production processes, clusters of larger blade-shaped samples were also cast in a commercial furnace at more moderate thermal gradients.

Ceramic molds for casting the cylindrical bars (1.3 cm. in diameter by 11.4 cm in length) were initially charged with 0.5 kg of alloy. The alloy was melted by resistance heating to approximately 1500ºC in the upper chamber of the modified Bridgman-type furnace. The directional solidification process was then initiated and controlled by withdrawal of the mold from the hot section of the furnace through a radiation baffle. Local solidification times were measured by inserting two thermocouples through the mold directly into the melt. The relationship between dendrite arm spacing and local solidification time was measured in a series of experiments by varying the withdrawal rates and local temperature gradient through adjustments in the gap between the mold and radiation baffle.

Blade-type castings were directionally solidified in cluster molds in a commercial furnace shown schematically in Figure 1. The superalloy charge was first induction melted at either 1482ºC or 1565ºC in the upper portion of the furnace and subsequently poured into a ceramic cluster mold seated on a copper chill plate. Again, control of power to the susceptor and the presence of the radiation baffle permitted a steep temperature gradient to be maintained at the solid-liquid interface. Blade samples were cast with the airfoil tip in contact with single crystal grain selector. One blade sample is shown in Figure 2, and it should be noted that the cross-sectional area of the base of the blade compared to the midspan of the airfoil is about three times larger. As with the cylindrical bars, local temperature gradients and withdrawal rates were varied and the breakdown of directional dendritic solidification studied. Solidification rates varying from 4.23×10^{-4} to 0.0113 cm/sec and temperature gradients at the solidification front covering the range of 0.3 - 140 ºC/cm were achieved.
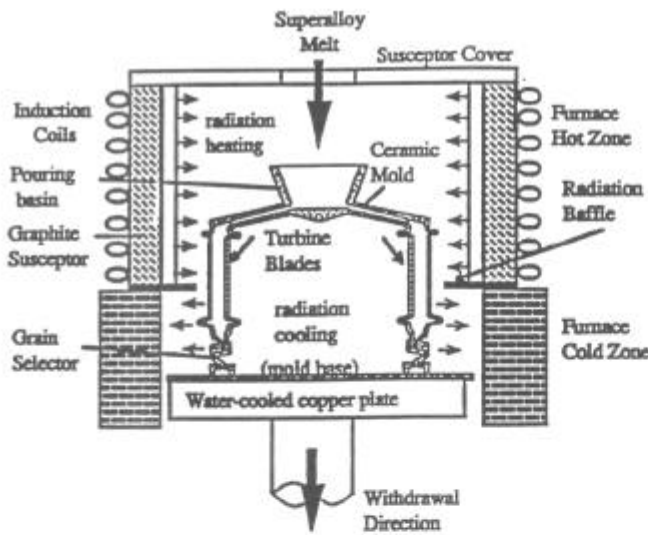

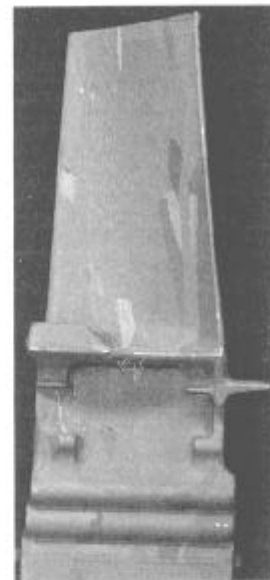Figure 1 - Schematic of commercial furnace used for directional solidification of cluster molds.

Figure 2 - Solid blade-shaped sample; note the isolated misoriented grains.

RESULTS

Three different behaviors which represent departures from single crystal solidification were found in these experiments. The general character of the three different types of grain defects will first be discussed. This will be followed by a detailed description of the alloy/process conditions which promoted formation of the grain defects, and then a discussion of the most likely mechanisms responsible for breakdown of single crystal solidification.

Types of Grain Defects

The first type of defect, shown in Figure 3, consists of small chains of equiaxed grains oriented parallel to the <001> solidification direction. These fine equiaxed grains, or "freckles" have been studied in detail by Giamei and co-workers [2, 3], and are associated with solute partitioning that progressively lowers the density of the liquid in the mushy zone, resulting in convective instabilities. Table II gives a comparison of the freckle composition to the average composition of interdendritic material (in areas of no freckling) for Alloy SX-1.

Table II - Composition (wt%) of Freckles Compared to Bulk Alloy and Average Interdendritic Composition

Material	Al	Cr	Co	Hf	Re	Ta	W	Ni
Nominal SX1	6.0	4.5	12.5	0.16	6.3	7.0	5.8	Bal
Interdendritic	7.6	4.4	12.2	0.13	3.4	8.2	3.9	Bal
Freckle	8.2	3.6	11.0	0.18	2.3	10.0	2.9	Bal

The freckles are strongly enriched in Ta and Al and depleted of Re and W, consistent with the view that they are formed from low density interdendritic liquid developed by solute partitioning. Average solute partition coefficients, k', expressed as the ratio of interdendritic to dendritic composition, are given for Alloy SX-1 in Table III. These results are in qualitative agreement with the segregation expected from Ni-X binaries and are similar to other superalloys [2, 4 - 6].

Table III - Average Solute Partition Ratios for Alloy SX1

$$k' = \frac{C_{dendritic}}{C_{interdendritic}} \quad (wt\%).$$

| Material	k'_{Al}	k'_{Cr}	k'_{Co}	k'_{Re}	k'_{Ta}	k'_{W}	k'_{Ni}
As-Cast SX-1	0.78	1.11	1.09	2.14	0.66	1.75	0.92

The second type of defect, shown in Figure 4, is a highly isolated misoriented "spurious" grain. These grains were generally much larger than freckle-type defects, usually several millimeters to a centimeter in extent. The misoriented grains were occasionally equiaxed in shape, but were more frequently somewhat elongated along the direction of growth with aspect ratios of 2:1 to 3:1. Microprobe analysis showed that the composition of the spurious grains did not differ significantly from the surrounding material. Nucleation could not be attributed to the presence of inclusions. However, as will be discussed further, nucleation and growth of misoriented grains was sensitive to alloy composition as well as processing conditions.

The third type of departure from single crystal solidification, shown in Figure 5, is a complete breakdown in the directional dendritic solidification process, similar to the "columnar to equiaxed" transition commonly found in large ingots [7 - 10]. In Figure 5 the transition has occurred as the solidification front moves into the thicker dovetail section of the blade where the thermal gradient is reduced by approximately 10%. Note also in Figure 5 that two isolated spurious grains have nucleated prior to the general transition.

Influence of Alloy Composition

A series of ten experiments with cluster molds containing 14 samples each were conducted at a constant growth rate (R) of 0.0113 cm/sec. The thermal gradient during solidification in the airfoil section of the samples was on average 10°C/cm. The influence of

alloy composition on the formation of freckle-type defects is summarized by Figure 6, where the average number of freckle chains per blade in each of the ten experiments is given. From Figure 6, the alloys most prone to freckle formation are SX-3, SX-4, SX-5 and SX-6, and SX-1. These alloys all contain higher levels of Re and/or W and low levels of Ta. Conversely, the alloys most resistant to freckling were alloys SX-7 and SX-8, which were high in Ta and low in Re and/or W.


1.0 mm
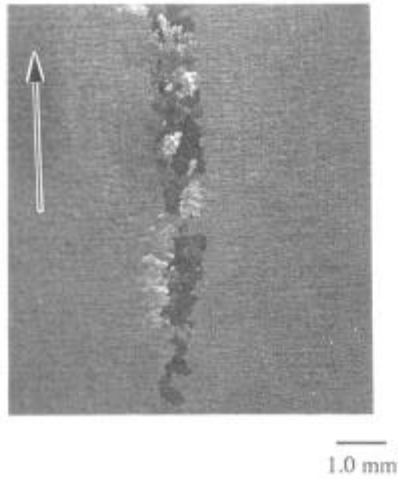
Figure 3 - Freckle chains formed during directional solidification. (Arrow marks solidification direction)

1.0 mm
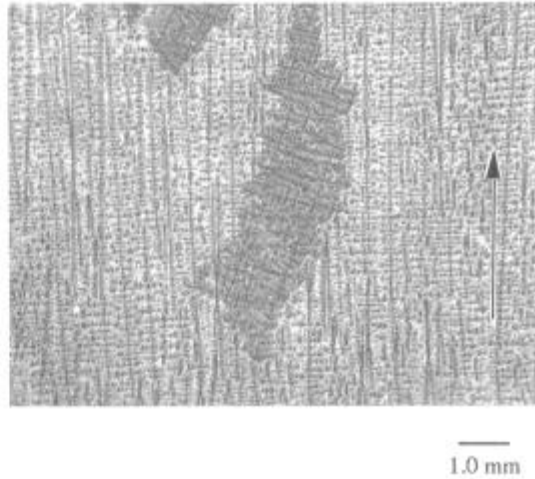
Figure 4 - An isolated "spurious" grain; dendrite traces show a high degree of misorientation. (Arrow marks solidification direction)

Statistical analysis of the data (analysis of variance) confirmed that Re, W and Ta significantly affected freckling, while the other alloying elements did not significantly influence the number of freckle chains (within this experimental range of compositions). From Table II it can be seen that these alloying elements are also the most strongly segregating and increase the density of the alloy. Increasing Ta can offset the effect of increasing Re and W since the Ta is rejected to the interdendritic areas as Re and W are depleted, decreasing the potential for density inversions.

Transition to
Equiaxed
Solidification

2.0 mm
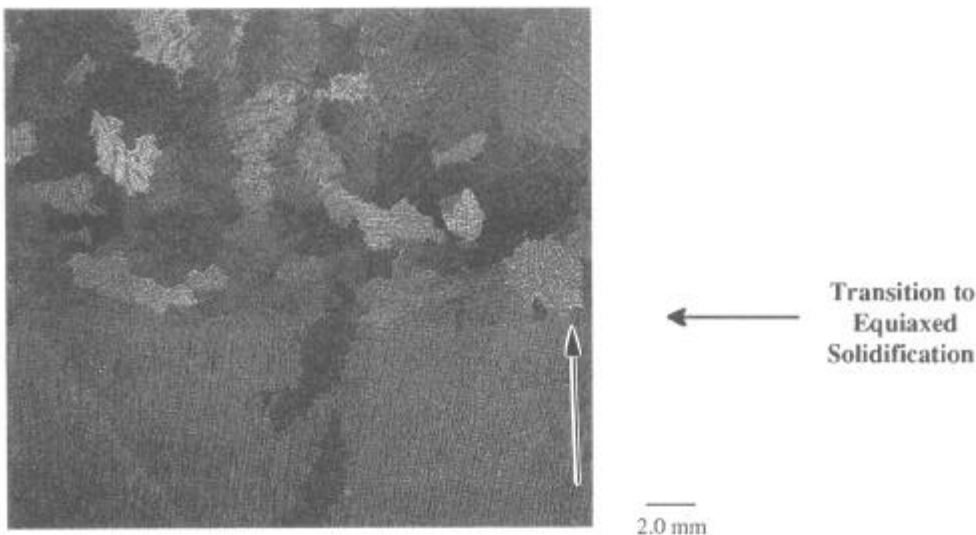
Figure 5 - An example of a general transition to completely equiaxed solidification.
(Arrow marks solidification direction)

129

The influence of alloy composition on the formation of misoriented grains is shown in Figure 7. Note that this data follows the same trend as for the freckling; as the levels of Re and W are increased or the Ta decreased, there is a greater potential for nucleation and growth of misoriented grains. As will be discussed further, these experiments suggest that solute-driven convective instabilities not only promote the nucleation and growth of freckles but also misoriented, "spurious" grains.
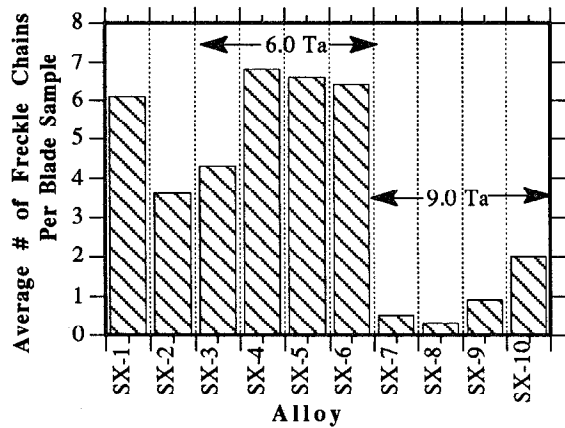

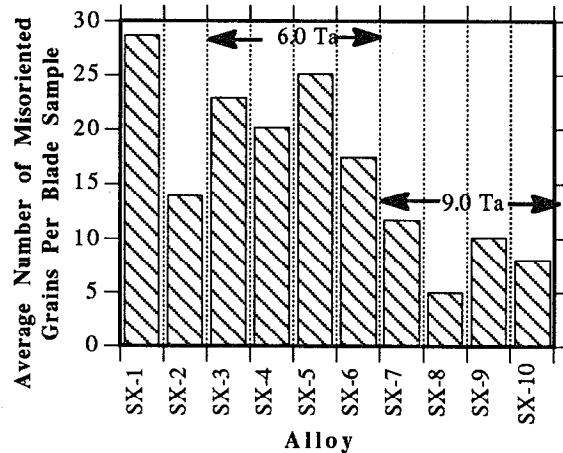Figure 6 - Influence of alloy content on freckle chain formation.

Figure 7 - Influence of alloy content on formation of misoriented grains.

Influence of Processing Conditions

To develop a better understanding of the externally imposed solidification conditions and the mechanisms associated with breakdown of single crystal solidification, Alloy SX-1 was chosen for further investigation. The relationship between dendrite arm spacing and local solidification time (cooling rate) was first established in a series of experiments with simple cylindrical bars. The results are shown in Figure 8 where Alloy SX-1 data is compared to the average behavior for eight other superalloys [11]. The cooling rate (G*R) was determined by calculating the average cooling rate between the equilibrium solidus and liquidus temperatures measured by the thermocouples inserted in the molds. Note that Alloy SX-1 is similar to other nickel base alloys, except for the low withdrawal rate (4.23×10^{-4} cm/sec) experiments. This difference in behavior at very low velocities, also noted by McLean [12], has been analyzed by Burden and Hunt [13], and is apparently related to the decreasing importance of radial concentration gradients as plane front solidification conditions are approached at very low solidification rates. At higher growth rates, the dendrite arm spacing follows the linear relationship in Figure 8 to dendrite arm spacings in excess of 300 μm.

Dendrite morphology as a function of cooling rate is shown in Figure 9, and it can be seen that as the cooling rate decreases, the primary arm spacing increases. At cooling rates below 0.1°C/sec, well defined tertiary arms begin to develop along the long secondary arms. As the dendrite arm spacing increased beyond 320μm, there were larger variations from the average spacing throughout the structure. The cooling rate data, supplemented with checks for consistency in the cluster molds was subsequently used for determination of the local temperature gradients in the more complicated blade geometries in a larger set of processing experiments which utilized solid blade-shaped samples cast in cluster molds.

A series of 25 experiments were conducted with cluster molds containing blades of Alloy SX-1. In these experiments, the imposed thermal gradients and solidification rates were varied over a wide range by adjusting mold withdrawal rates, number of blades on a cluster mold, amount of superheat prior to pouring the alloy onto the chill plate, and by making minor adjustments in the furnace configuration which influenced the heating and cooling efficiency in

the vicinity of the radiation baffle. Withdrawal rates varied from 5.6×10^{-3} cm/sec to 0.0127 cm/sec and temperature gradients varied from 0.3 to 23 °C/cm. After each experiment, grain defects on each blade were thoroughly mapped and characterized according to size and location. Only the results in terms of average numbers of grain defects per blade will be given here; these average numbers were found to be representative of the more detailed treatments of the data (numbers of defects in the airfoils, dovetails, etc.).
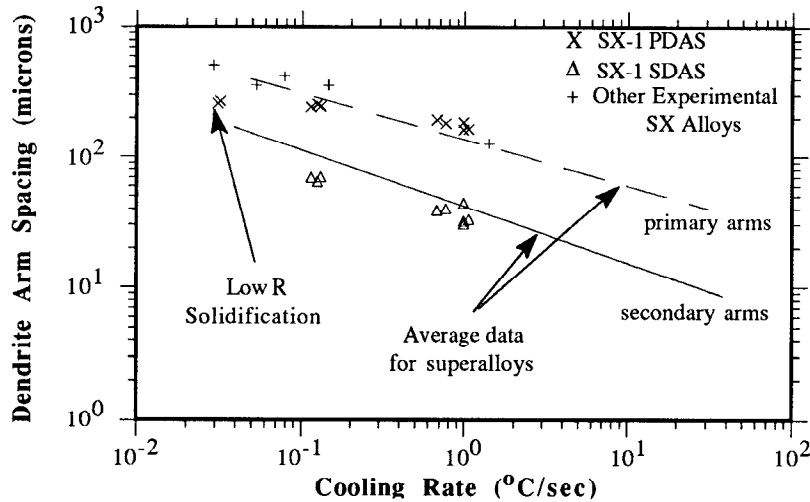
Figure 8 - Relationship of dendrite arm spacings to cooling rate during solidification for Alloy SX-1 compared to the average data for other superalloys [11].

Results for the number of freckle chains formed as a function of dendrite arm spacing are given in Figure 10. Below a critical dendrite arm spacing of about 320μm the formation of freckle-type defects is suppressed in Alloy SX-1. This corresponds to a critical cooling rate of approximately 0.1°C/sec, as shown in Figure 8. The number of misoriented grains as a function of dendrite arm spacing is shown in Figure 11. From this, three different regimes of behavior can be defined according to the type of grain defect and primary dendrite arm spacing. In the first regime, at spacings less than 320 μm, there is directional dendritic solidification with no misoriented grains (or freckles). In the second regime, at spacings between 320 μm and about 600μm, isolated misoriented misoriented grains (as well as freckles) are formed. In Regime III there is a complete transition to equiaxed solidification. For a given solidification rate, for example R=0.0113 cm/sec, the transition from Regime I to II occurs at a thermal gradient of 8°C/cm and from II to III around 1.4°C/cm. These transitions cannot be clearly defined to occur at critical levels of G or G/R, and this is apparently due to the fact that solute-driven convection is more important to nucleation of all of the grain defects than constitutional supercooling or heterogeneous nucleation of equiaxed grains, which have also been suggested as mechanisms for the columnar to equiaxed transition [7 - 9].

Mechanism of Grain Nucleation
        As mentioned in the previous section, misoriented grains may form when the primary dendrite arm spacing exceeds 320 μm, corresponding (Figure 8) to a local cooling rate of approximately 0.1°C/sec. Below this critical cooling rate there is also a transition in dendrite morphology (Figure 9), with the development of significant numbers of tertiary arms. At increasingly lower gradients the tertiary arms become more prominent, and may extend over distances of several hundred microns. Another microstructural feature associated with the Regime II and III processing conditions was the presence of fragmented secondary and tertiary dendrite arms. In Figure 12, a plane normal to the solidification direction shows a secondary arm which has remelted and separated from the primary trunk of the dendrite, and is also "bent"

131

away from its characteristic <010> crystallographic orientation. In Figure 13, viewing a surface plane parallel to the solidification direction, it can also be seen that a separated secondary dendrite arm has served to nucleate a grain at the dendritic/equiaxed interface. This microstructural evidence coupled with the observation that heavily segregating solute elements promote convective instabilities as well as formation of misoriented grains, suggests that dendrite fragmentation is responsible for nucleation of misoriented grains. In transparent model compounds [10, 14] dendrite remelting and large differences in dendrite morphology as a function of gravity level have been detected, demonstrating the important influence of convection on the development of dendritic structure. Since interdendritic fluid flow due to density differences in the liquid is sensitive to dendrite arm spacing [15], the onset of freckling and nucleation of spurious grains at the same critical dendrite arm spacing of 320μm in Alloy SX-1 is further evidence that solute-driven convection is responsible for the formation of both types of defects.

PDAS = 166 microns
G*R = 0.77 °C/sec

PDAS = 294 microns
G*R = 0.13 °C/sec

PDAS = 361 microns
G*R = 0.07 °C/sec
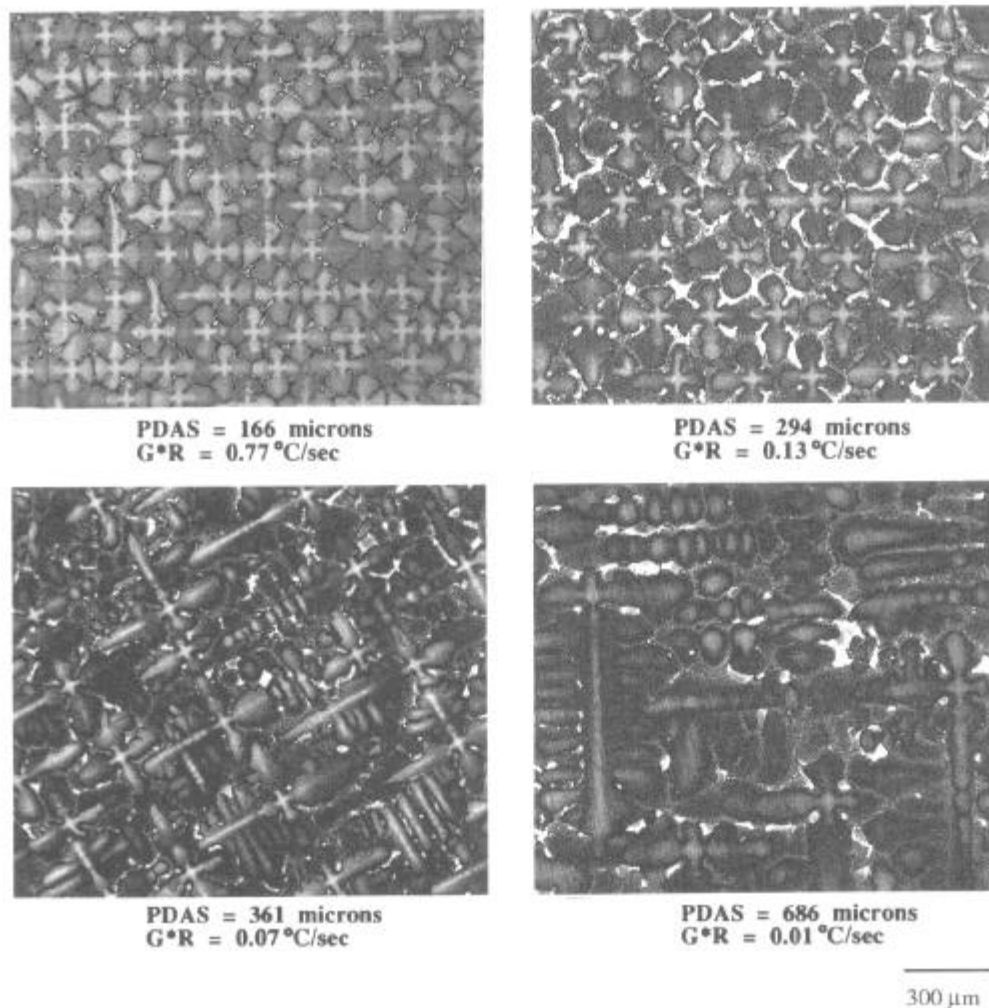
PDAS = 686 microns
G*R = 0.01 °C/sec

300 μm

Figure 9 - Variations in dendrite morphology with cooling rate during directional solidification of Alloy SX-1.

For the misoriented grains, the nucleation events were infrequent for a moderately positive thermal gradient ahead of the dendrite tips; this is probably due to complete remelting of most of the fragmented dendrites. For a fixed solidification rate, as the local thermal gradients become very low (approaching conditions of unconstrained solidification), there is apparently an abundance of fragmented dendrites that do not remelt, resulting in a general columnar to equiaxed transition. It is of interest to note that unless the transition is studied with single

crystals rather than by columnar polycrystals, that it may be difficult to detect an occasional misoriented grain nucleation event which precedes the general columnar to equiaxed transition.
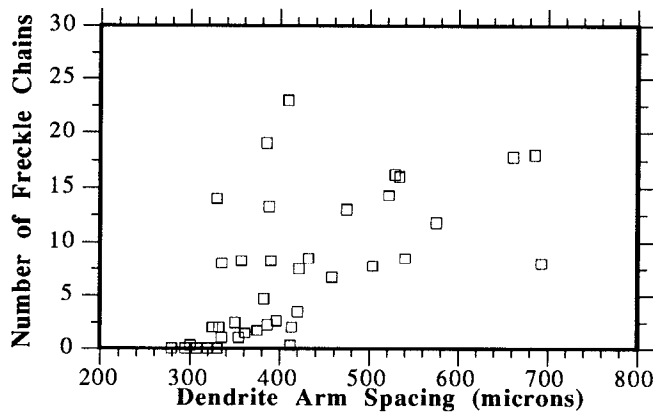

Figure 10 - Dependence of freckle formation on dendrite arm spacing. The critical spacing of 320μm corresponds to a cooling rate (G*R) of 0.1°C/sec.
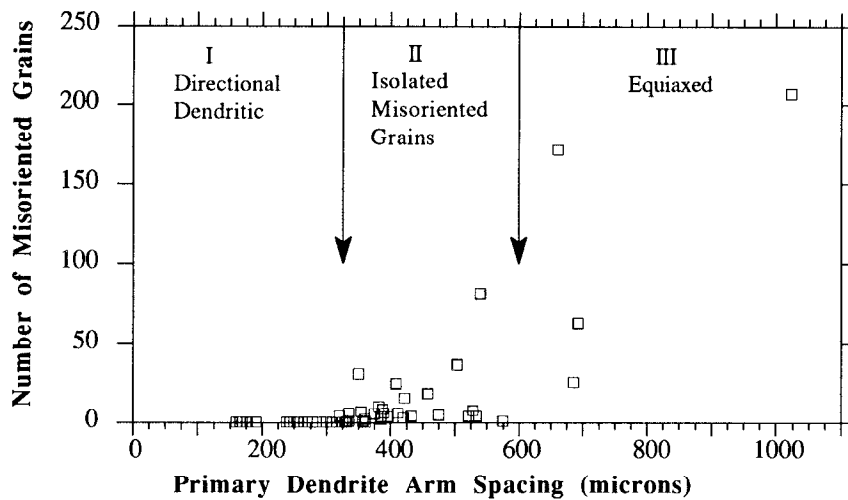
Figure 11 - The three regimes of grain defect formation and the dependence on dendrite arm spacing.

SUMMARY

Grain defect formation during directional solidification of nickel base single crystals has been studied for a wide range of alloy and process conditions. Partitioning of Re, W, and Ta during solidification leads to the development of convective instabilities which promote freckling and equiaxed grain nucleation through dendrite fragmentation. In Alloy SX-1 the onset of freckling as well nucleation of isolated misoriented grains occurs at a critical cooling rate of 0.1°C/sec. This transition in solidification behavior also corresponds to a transition in dendrite morphology with the development of many tertiary arms at the critical primary dendrite arm spacing of 320μm. As the thermal gradients at the solidification front are further reduced, a complete transition to equiaxed solidification occurs, and for Alloy SX-1 this transition occurs for a primary arm spacing of approximately 600μm.

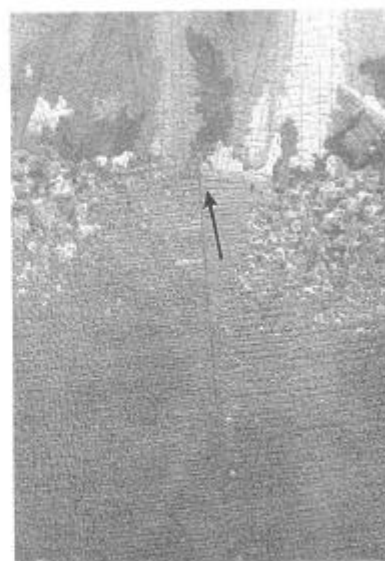equiaxed & columnar grains

transition →

single crystal

200 µm
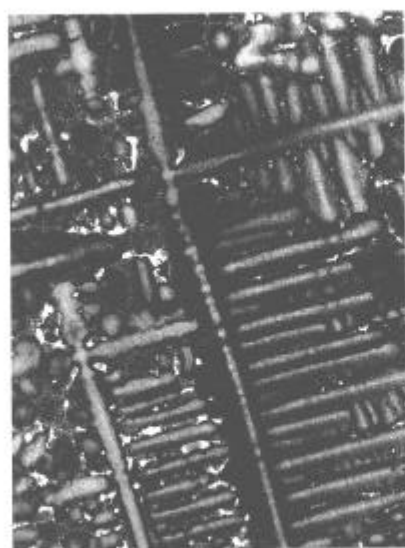
1.0 mm

Figure 12 - Detachment of secondary and tertiary dendrite arms. (Viewed normal to the solidification direction.)

Figure 13 - Separation of a secondary dendrite arm at the transition to equiaxed solidification. (Viewed parallel to the solidification direction at the sample surface.)

ACKNOWLEDGEMENTS

REFERENCES

1. D.N. Duhl in *Superalloys, Supercomposites and Superceramics*, ed. by J.K. Tien and T. Caulfield, Academic Press, Boston, (1988).
2. A.F. Giamei and B.H. Kear, *Metall. Trans.* **1A**, 2185, (1970).
3. S.M. Copley, A.F. Giamei, S.M. Johnson, and M.F. Hornbecker, *Metall. Trans.* **1A**, 2193, (1970).
4. S.N. Tewari, M. Vijaya Kumar, J.E. Lee, and P.A. Curreri, NASA TM-103518, (1990).
5. R.M. Sharp and M.C. Flemings, *Metall. Trans.* **4B**, 997, (1973).
6. H. Biloni and G.F. Bolling, *Trans. AIME* **227**, 1351, (1963).
7. B. Chalmers in *Principles of Solidification*, Krieger, New York, (1977).
8. J.D. Hunt, *Mater. Sci. Eng.* **65**, 75, (1984).
9. W.C. Winegard and B. Chalmers, *Trans. ASM*, **46**, 1214, (1954).
10. K.A. Jackson, J.D. Hunt, D.R. Uhlmann and T.P. Seward, *Trans. AIME* **236**, 149, (1966).
11. G.K. Bouse and J.R. Mihalisin in *Superalloys, Supercomposites and Superceramics*, ed. by J.K. Tien and T. Caulfield, Academic Press, Boston, (1988).
12. P.N. Quested and M. McLean, *Mater. Sci. Eng.* **65**, 171, (1984).
13. M.H. Burden and J.D. Hunt, *J. Crystal Growth* **22**, 109, (1974).
14. M.H. Johnston and C.S. Griner, *Metall. Trans.* **8A**, 77, (1977).
15. A.K. Sample and A. Hellawell, *Metall. Trans.* **15A**, 2163, (1984).